

Preparation of Ga_2O_3 thin film solar-blind photodetectors based on mixed-phase structure by pulsed laser deposition

Y M Lu(吕有明), C Li(李超), X H Chen(陈相和), S Han(韩瞬), P J Cao(曹培江), F Jia(贾芳), Y X Zeng(曾玉祥), X K Liu(刘新科), W Y Xu(许望颖), W J Liu(柳文军), D L Zhu(朱德亮)

Citation: Chin. Phys. B . 2019, 28(1): 018504. **doi:** 10.1088/1674-1056/28/1/018504
Journal homepage: http://cpb.iphy.ac.cn; http://iopscience.iop.org/cpb

What follows is a list of articles you may be interested in

Integration of a field-effect-transistor terahertz detector with a diagonal horn antenna

Xiang Li(李想), Jian-dong Sun(孙建东), Zhi-peng Zhang(张志鹏), V V Popov, Hua Qin(秦华)

Chin. Phys. B . 2018, 27(6): 068506. **doi:** 10.1088/1674-1056/27/6/068506

Performance of dual-band short- or mid-wavelength infrared photodetectors based on InGaAsSb bulk materials and InAs/GaSb superlattices

Yao-yao Sun(孙姚耀), Yue-xi Lv(吕粤希), Xi Han(韩玺), Chun-yan Guo(郭春妍), Zhi Jiang(蒋志), Hong-yue Hao(郝宏玥), Dong-wei Jiang(蒋洞微), Guo-wei Wang(王国伟), Ying-qiang Xu(徐应强), Zhi-chuan Niu(牛智川)

Chin. Phys. B . 2017, 26(9): 098506. **doi:** 10.1088/1674-1056/26/9/098506

Very long wavelength infrared focal plane arrays with 50% cutoff wavelength based on type-II InAs/GaSb superlattice

Xi Han(韩玺), Wei Xiang(向伟), Hong-Yue Hao(郝宏玥), Dong-Wei Jiang(蒋洞微), Yao-Yao Sun(孙姚耀), Guo-Wei Wang(王国伟), Ying-Qiang Xu(徐应强), Zhi-Chuan Niu(牛智川)

Chin. Phys. B . 2017, 26(1): 018505. **doi:** 10.1088/1674-1056/26/1/018505

High-speed waveguide-integrated Ge/Si avalanche photodetector

Hui Cong(丛慧), Chunlai Xue(薛春来), Zhi Liu(刘智), Chuanbo Li(李传波), Buwen Cheng(步成文), Qiming Wang(王启明)

Chin. Phys. B . 2016, 25(5): 058503. **doi:** 10.1088/1674-1056/25/5/058503

Design and fabrication of multi-channel photodetector array monolithic with arrayed waveguide grating

Qian-Qian Lv(吕倩倩), Pan Pan(潘盼), Han Ye(叶焓), Dong-Dong Yin(尹冬冬),Yu-Bing Wang(王玉冰), Xiao-Hong Yang(杨晓红), Qin Han(韩勤)

Chin. Phys. B . 2016, 25(3): 038505. **doi:** 10.1088/1674-1056/25/3/038505

SPECIAL TOPIC — Photodetector: Materials, physics, and applications

Preparation of Ga_2O_3 thin film solar-blind photodetectors based on mixed-phase structure by pulsed laser deposition*

Y M Lu(吕有明)†, C Li(李超), X H Chen(陈相和), S Han(韩瞬), P J Cao(曹培江), F Jia(贾芳), Y X Zeng(曾玉祥), X K Liu(刘新科), W Y Xu(许望颖), W J Liu(柳文军), and D L Zhu(朱德亮)

College of Materials Science and Engineering, Shenzhen Key Laboratory of Special Functional Materials, Shenzhen Engineering Laboratory for Advanced Technology of Ceramics, Guangdong Research Center for Interfacial Engineering of Functional Materials, Shenzhen University, Shenzhen 518060, *China*

(Received 22 August 2018; revised manuscript received 7 November 2018; published online 12 December 2018)

Gallium oxide (Ga_2O_3) thin films were deposited on a-Al_2O_3 ($11\bar{2}0$) substrates by pulsed laser deposition (PLD) with different oxygen pressures at 650 °C. By reducing the oxygen pressure, mixed-phase Ga_2O_3 films with α and β phases can be obtained, and on the basis of this, mixed-phase Ga_2O_3 thin film solar-blind photodetectors (SBPDs) were prepared. Comparing the responsivities of the mixed-phase Ga_2O_3 SBPDs and the single β-Ga_2O_3 SBPDs at a bias voltage of 25 V, it is found that the former has a maximum responsivity of approximately 12 A/W, which is approximately two orders of magnitude larger than that of the latter. This result shows that the mixed-phase structure of Ga_2O_3 thin films can be used to prepare high-responsivity SBPDs. Moreover, the cause of this phenomenon was investigated, which will provide a feasible way to improve the responsivity of Ga_2O_3 thin film SBPDs.

Keywords: Ga_2O_3, mixed-phase, solar-blind photodetector, pulsed laser deposition

PACS: 85.60.Gz, 81.15.Fg, 81.10.Pq **DOI:** 10.1088/1674-1056/28/1/018504

1. Introduction

Recently, solar-blind photodetectors (SBPDs) based on wide-bandgap semiconductors (e.g. Ga_2O_3,[1–5] GaN,[6,7] $Al_xGa_{1-x}N$,[8,9] BN,[10] diamond,[11,12] and $Zn_{1-x}Mg_xO$[13]) have been extensively investigated owing to their wide range of civil and military applications, such as biomedical applications, flame detection, missile tracking, and intersatellite communication. However, for the $Al_xGa_{1-x}N$ photodetectors that have been prepared, the device performance easily degrades as the Al concentration increases. The main drawback of BN and diamond is that their bandgaps are too large, approximately 6.3 eV and 5.5 eV, respectively, which makes their absorption edges fall at short wavelengths of 193 nm and 225 nm. Therefore, the full solar-blind UV wavelength cannot be effectively detected. For ZnMgO SBPDs,[14–17] the main drawbacks of wurtzite ZnMgO (w-ZMO) and cubic ZnMgO (c-ZMO) are the relatively large dark current and low responsivity, respectively. Fortunately, high-performance SBPDs based on mixed-phase ZnMgO (m-ZMO) thin films have been recently reported, and these devices possess a dark current of 78 pA and a photoresponsivity of 434 A/W,[15] which may be due to the large amounts of heterojunction interfaces between w-ZMO and c-ZMO. However, to obtain a high-performance m-ZMO SBPD, the Mg content of the film must be accurately controlled, which increases the difficulty of preparing the eligible film and device. Nevertheless, these results still provide a viable idea that better-performance SBPDs can be fabricated on gallium oxide (Ga_2O_3) thin films with mixed-phase structures.

It is surprising that among these materials, Ga_2O_3, which has a bandgap (E_g) of 4.4–5.15 eV, is intrinsically suitable for solar-blind photodetection. Amorphous Ga_2O_3 is easily prepared and has great potential for high-performance photodetection; therefore, it has received extensive attention. For instance, Kumar *et al.*[18] comprehensively investigated the structure, morphology, and optical properties of amorphous Ga_2O_3 thin films. Qian *et al.*[1] showed that the metal–semiconductor–metal (MSM) SBPD based on an amorphous Ga_2O_3 thin film has a responsivity as high as 70.26 A/W; this is because the amorphous Ga_2O_3 film possesses a high density of defects, oxygen vacancies, dangling bonds, etc., which contribute to the high internal gain. However, both the defects and oxygen vacancies act as trap centers and capture the photogenerated carriers, and thus hinder the recombination of hole–electron pairs, which would lead to persistent photoconductivity and ultimately a longer recovery time. Therefore, much of the work so far has focused on crystallized Ga_2O_3 thin films. Ga_2O_3 has five crystal structure phases, α, β, δ, ε,

*Project supported by the National Natural Science Foundation of China (Grant Nos. 51872187, 51302174, 11774241, and 61704111), the National Key Research and Development Program of China (Grant No. 2017YFB0400304), the Natural Science Foundation of Guangdong Province, China (Grant Nos. 2016A030313060 and 2017A030310524), the Project of Department of Education of Guangdong Province, China (Grant No. 2014KTSCX110), the Fundamental Research Project of Shenzhen, China (Grant No. JCYJ20180206162132006), and the Science and Technology Foundation of Shenzhen, China (Grant No. JCYJ2015-2018).

†Corresponding author. E-mail: ymlu@szu.edu.cn

© 2019 Chinese Physical Society and IOP Publishing Ltd

and γ.[19] Among these five phases, monoclinic β-Ga_2O_3 has attracted much attention and been extensively investigated due to its good physical, chemical, and thermal stability. Additionally, the bandgap width of β-Ga_2O_3 is approximately 4.9 eV, corresponding to an absorption edge of approximately 250–280 nm, thus enabling effective detection of the whole solar-blind UV wavelength.[20–22] For example, Yu *et al.*[4] fabricated a β-Ga_2O_3 MSM SBPD with excellent performance by pulsed laser deposition (PLD) at 800 °C; the device possessed a very low dark current of approximately 1.2×10^{-11} A, but a lower responsivity of 0.903 A/W. Interestingly, corundum α-Ga_2O_3 has a wider bandgap than β-Ga_2O_3, which is approximately 5.15 eV, and is intrinsically suitable for solar-blind photodetection. Recently, Guo *et al.*[23] reported a device with an MSM structure based on an α-Ga_2O_3 thin film, and investigated the UV photoresponse characteristics. The α-Ga_2O_3 SBPD possessed a very low dark current, but the responsivity was also relatively low. Consequently, it can be seen that the performance of both β-Ga_2O_3 and α-Ga_2O_3 SBPDs, such as the responsivity, remains lower than expected.[4,24] To achieve a better performance in solar-blind photodetection, we employed the idea of preparing m-ZMO SBPDs; therefore, several mixed-phase Ga_2O_3 SBPDs were prepared, and the optoelectrical properties of the SBPDs were definitively studied.

In this work, we explored the growth of Ga_2O_3 thin films on a-Al_2O_3 substrates under various oxygen pressures at 650 °C by PLD. Then, MSM SBPDs based on β-Ga_2O_3 and mixed-phase Ga_2O_3 thin films were fabricated. The UV photoresponse characteristics of the devices were analyzed in detail.

2. Experimental details

Ga_2O_3 thin films were grown on a-Al_2O_3 $(11\bar{2}0)$ by the PLD technique using a KrF laser ($\lambda = 248$ nm) with a repetition rate of 2 Hz and a laser energy of 300 mJ. A stoichiometric ceramic Ga_2O_3 target (99.99% purity) with a 29.6 mm diameter was used for the Ga_2O_3 thin film deposition. The substrate was kept 60 mm away from the target, and the substrate was fixed at 650 °C during film growth. When the deposition chamber was pumped to a base pressure below 6.0×10^{-4} Pa, oxygen gas (99.999%) was introduced into the chamber, and the deposition oxygen pressure was maintained at 3.0 Pa, 2.0 Pa, 1.0 Pa, 0.5 Pa, or 0.09 Pa. The oxygen flow rate and the growth time of the Ga_2O_3 films were fixed at 30 sccm and 60 min, respectively, for all samples. After deposition, all the samples were naturally cooled down to 80 °C at a base pressure of 6.0×10^{-4} Pa, and then removed from the chamber. The thickness of the Ga_2O_3 layer was measured by an ET-4000M model high-precision probe profiler manufactured by Japan Kosaka Corporation. The crystal structure and quality of the films were investigated by x-ray diffraction (XRD) (D8 Advance SS 18KW) with Cu K_α radiation ($\lambda = 1.5418$ Å) as the x-ray source, and the structure of the Ga_2O_3 thin films was also confirmed by Raman spectroscopy. The transmittance spectra of the Ga_2O_3 films were analyzed by a UV–visible spectrophotometer (UV-2450) in the wavelengths ranging from 200 nm to 600 nm. The surface morphology of the film was characterized by field emission scanning electron microscopy (SEM, SU-70).

The process of preparing the SBPDs with an interdigitated MSM structure was as follows: a Au (50 nm) film was grown on the surface of the Ga_2O_3 film by thermal evaporation, finally forming a Schottky contact. Afterward, electrodes with an interdigitated structure were fabricated using standard photolithography and wet etching processes. Both the finger width and the interspacing were 10 μm, and the finger length was 500 μm. After fabrication of the device, several performance characteristics were analyzed. Spectral responsivity measurements were carried out using a Zolix solar cell scan 100 measurement system with a 150 W xenon lamp as the light source. In addition, a Keithely 2450 was used as a bias source for testing the photoresponsivity of the device under different bias voltages.

3. Results and discussion

Figure 1 shows the XRD (θ–2θ) patterns of the Ga_2O_3 films grown on a-Al_2O_3 $(11\bar{2}0)$ substrates at various oxygen pressures. When the oxygen pressure decreases from 3.0 Pa to 2.0 Pa, the a-Al_2O_3 $(11\bar{2}0)$ diffraction peak and the characteristic diffraction peaks of $(\bar{2}01)$, (400), $(\bar{6}01)$, $(\bar{6}03)$, and $(\bar{8}01)$ belonging to the monoclinic phase of β-Ga_2O_3 films are observed, but no characteristic diffraction peak of α-Ga_2O_3 films is observed. However, upon further decreasing the oxygen pressure to 1.0 Pa, in addition to the aforementioned diffraction peaks, the characteristic (110) diffraction peak of α-Ga_2O_3 films also appears, which is consistent with the result reported in the literature that α-Ga_2O_3 can be grown on a-Al_2O_3 substrates.[25] It is worth noting that when the oxygen pressure is further decreased to 0.5 Pa and 0.09 Pa, the results are basically the same as for the sample grown with an oxygen pressure of 1.0 Pa, which indicates that the mixed-phase Ga_2O_3 film with coexisting β-Ga_2O_3 and α-Ga_2O_3 can be obtained on an a-Al_2O_3 substrate. In addition, the intensities of the (400) and $(\bar{2}01)$ diffraction peaks are the strongest for the 1.0 Pa sample among all of the mixed-phase Ga_2O_3 thin films. The specific reason for this phenomenon will be further explained in detail below.

Generally, regarding the crystal growth orientation of semiconductor material,[26–28] the higher the dangling bond density of a certain crystal plane, the greater the attraction

force to reactive atoms and the smaller the energy of reactive atoms that can migrate to this type of crystal surface. Conversely, if the dangling bond density of a certain crystal plane is smaller, then the ability to attract reactive atoms is weaker, and only the atoms with a large migration energy can migrate to the surface of this type of crystal plane. Figure 2(a) shows a diagram of the β-Ga_2O_3 unit cell; the atomic arrangements of the $(\bar{4}02)$ and (400) planes belonging to β-Ga_2O_3 are also displayed. The atomic density of the β-Ga_2O_3 (400) crystal plane is calculated as 14.462 nm^{-2} by referring to the atomic arrangement of (400), and there are three dangling bonds around each atom according to the diagram of the β-Ga_2O_3 unit cell; therefore, the dangling bond density on the surface of the β-Ga_2O_3 (400) plane is 34.384 nm^{-2}. Similarly, the atomic density of the β-Ga_2O_3 $(\bar{4}02)$ plane is calculated as 13.867 nm^{-2} by referring to the atomic arrangement of $(\bar{4}02)$, and there are three dangling bonds around each atom according to the diagram of the β-Ga_2O_3 unit cell; therefore, the dangling bond density on the surface of the β-Ga_2O_3 $(\bar{4}02)$ plane is 41.601 nm^{-2}.

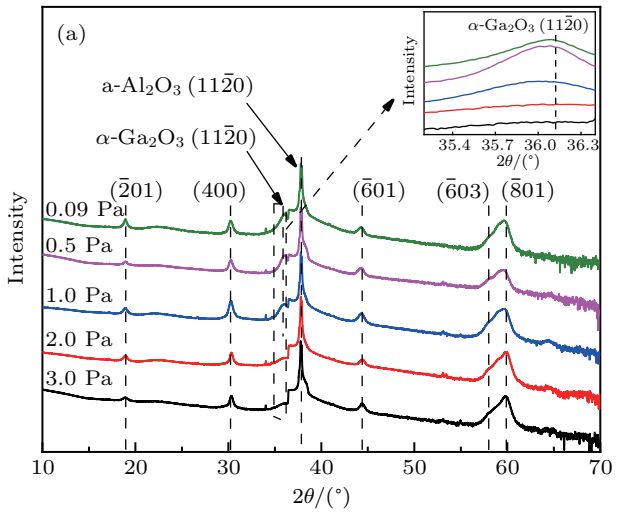


Fig. 1. The XRD (θ–2θ) patterns of the Ga_2O_3 films with various oxygen pressures (3.0–0.09 Pa) grown on a-Al_2O_3 $(11\bar{2}0)$ substrates; the inset is the partial enlargement of the XRD patterns.

Figure 3(b) shows a diagram of the α-Ga_2O_3 unit cell and the atomic arrangement of the (110) plane. According to Fig. 3(b), the number of dangling bonds around each atom is three, and the atomic and dangling bond densities of the α-Ga_2O_3 (110) plane are 10.157 nm^{-2} and 30.471 nm^{-2}, respectively. The dangling bond densities of these three crystal planes are ranked in ascending order as follows: β-Ga_2O_3 $(\bar{4}02)$ > β-Ga_2O_3 (400) > α-Ga_2O_3 (110). Therefore, theoretically, the order of the three crystal planes in terms of the atomic attraction to reactive atoms is β-Ga_2O_3 $(\bar{4}02)$ > β-Ga_2O_3 (400) > α-Ga_2O_3 (110). The attraction force of the α-Ga_2O_3 (110) plane is the weakest, which implies that the growth of the α-Ga_2O_3 (110) plane requires higher migration energy. Both the probability of atoms colliding with each other and the number of collisions are small when the oxygen pressure in the chamber is low. As a result, more reactive atoms from the target can reach the surface of the substrate and migrate to the α-Ga_2O_3 (110) plane. In contrast, fewer Ga and O atoms from the target can reach the surface of the substrate and migrate to the α-Ga_2O_3 plane when the oxygen pressure in the chamber is high. It should be noted that this indicates good agreement between our research result and the theory of crystal growth. Coincidentally, the experimental method for and the theory of this difference in structure growth have been reported in the relevant literature for the growth of ZnMgO thin films.[29]

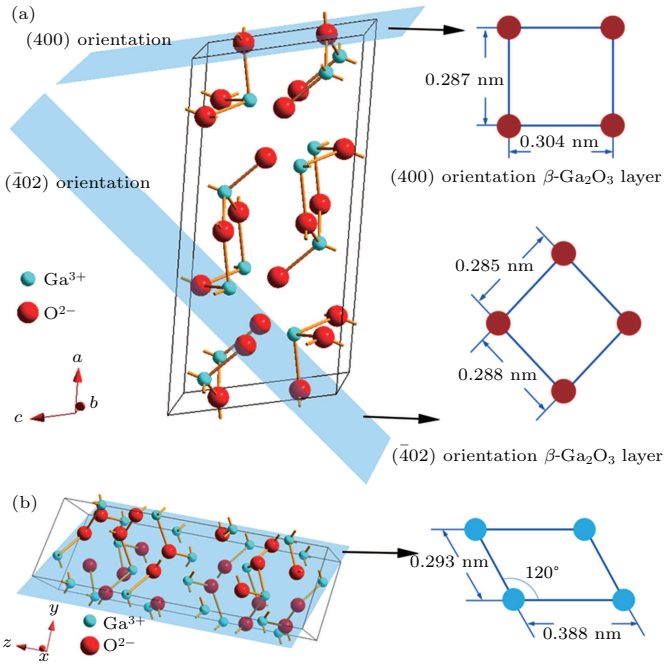


Fig. 2. (a) Diagram of β-Ga_2O_3 unit cell, and the atomic arrangement of (400) and $(\bar{4}02)$ planes; (b) diagram of α-Ga_2O_3 unit cell, and the atomic arrangement of the (110) plane.

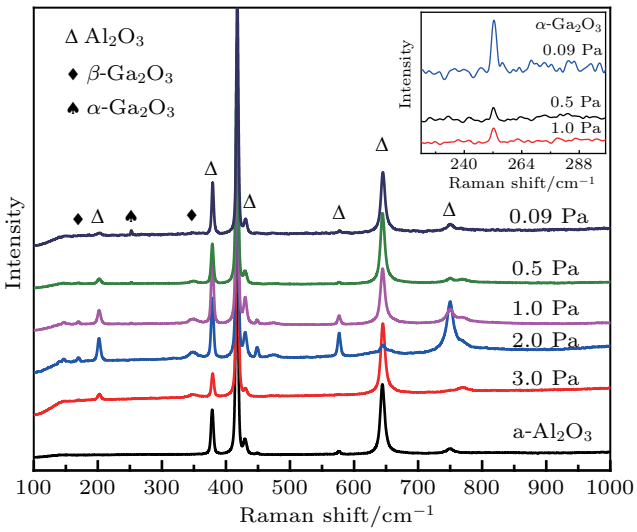


Fig. 3. Raman spectra of Ga_2O_3 thin films with various oxygen pressures grown on a-plane a-Al_2O_3 $(11\bar{2}0)$ substrates. The inset is the partial enlargement of the samples of 1.0 Pa, 0.5 Pa, and 0.09 Pa.

To further confirm that the Ga_2O_3 thin film is present in the form of a mixed-phase structure with coexisting α and β phases when the oxygen growth pressure does not exceed 1.0 Pa, Raman spectrum measurements were performed. Figure 3 shows the Raman spectra of Ga_2O_3 thin films grown with various oxygen pressures on a-Al_2O_3 ($11\bar{2}0$) substrates. The inset displays a partial enlargement for the 1.0 Pa, 0.5 Pa, and 0.09 Pa samples. It can be clearly seen that the characteristic Raman peaks of β-Ga_2O_3 films appear at 170 cm^{-1}, 200 cm^{-1}, and 350 cm^{-1}.[30,31] Interestingly, in addition to the aforementioned characteristic Raman peaks belonging to the β-Ga_2O_3 film, another Raman peak for the Ga_2O_3 film appears at 251 cm^{-1}. According to the literature,[32] β-Ga_2O_3 films have no Raman peaks within 200–300 cm^{-1}, and therefore the Raman peak at 251 cm^{-1} belongs to α-Ga_2O_3. The same results are obtained when the oxygen pressure is further reduced to a pressure of 0.5 Pa or 0.09 Pa. This is consistent with the observation from XRD patterns. On the basis of this result, it can be confirmed that by reducing the oxygen growth pressure, it is possible to grow a mixed-phase Ga_2O_3 thin film with coexisting α-Ga_2O_3 and β-Ga_2O_3.

SEM was used to further elucidate the relationship between the surface morphology and crystal orientation. Figure 4 shows the SEM images of the Ga_2O_3 thin films grown at various oxygen pressures, with a magnification of 35 K. It can be clearly seen that the surface morphologies of the Ga_2O_3 thin films grown at 0.09 Pa, 0.5 Pa, and 1.0 Pa are rougher than those at 2.0 Pa and 3.0 Pa, which could be because the latter exhibit a single phase. The results are consistent with the observed XRD patterns and Raman spectra. Obviously, the result suggests that the surface morphology of the Ga_2O_3 thin film is rougher when the Ga_2O_3 thin film is mixed-phase because the growth rates of different crystal orientations are discrepant.

Figure 5 shows the absorbance spectrum of the Ga_2O_3 thin films deposited at different oxygen pressures, where the substrate temperature was 650 °C. The inset is the $(\alpha h\nu)^2$ versus $h\nu$ plot of Ga_2O_3 films grown with different oxygen pressures. It is evident that all the Ga_2O_3 thin films have a significant absorption cut-off edge, which is located at 250–300 nm. A further analysis of the optical spectra was performed to calculate the energy bandgap. For α and β phase Ga_2O_3 with a direct bandgap, the absorption follows the power law:[2,33]

$$(\alpha h\nu)^2 = k(h\nu - E_g), \tag{1}$$

where α is the absorption coefficient, $h\nu$ is the energy of the incident photon, k is a constant, and E_g is the bandgap. The optical absorption coefficient α of the film is evaluated using the formula below:[33]

$$\alpha = \ln(100/T)/d, \tag{2}$$

where T is the transmittance of the thin film, and d is the thickness of the thin film. The optical bandgap is determined by extrapolating the linear region of the plot $(\alpha h\nu)^2$ versus $h\nu$ and taking the intercept on the $h\nu$ axis. As shown in the illustration, when the oxygen pressure is reduced from 3.0 Pa to 2.0 Pa, the optical bandgap of the Ga_2O_3 thin films changes quite slightly due to their same single β phase. However, the optical bandgap of the Ga_2O_3 thin films changes significantly and by a larger amount compared to the former films when the oxygen pressure is decreased from 1.0 Pa to 0.09 Pa. The main reason for this phenomenon is that all the films are mixed-phase Ga_2O_3, and the lower the oxygen pressure, the higher the proportion of α-Ga_2O_3.

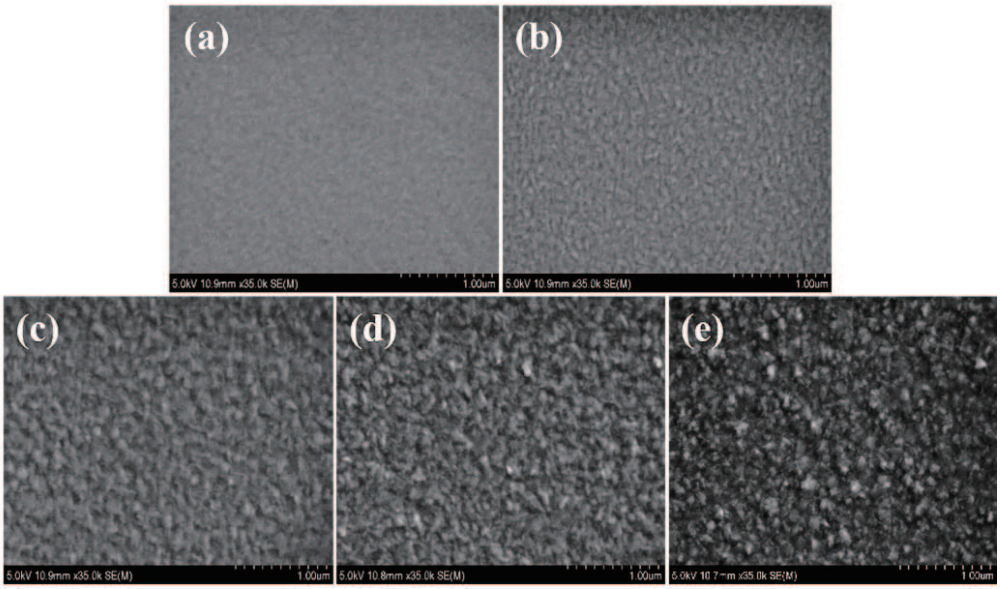


Fig. 4. SEM images of Ga_2O_3 thin films: (a) 3.0 Pa, (b) 2.0 Pa, (c) 1.0 Pa, (d) 0.5 Pa, (e) 0.09 Pa.

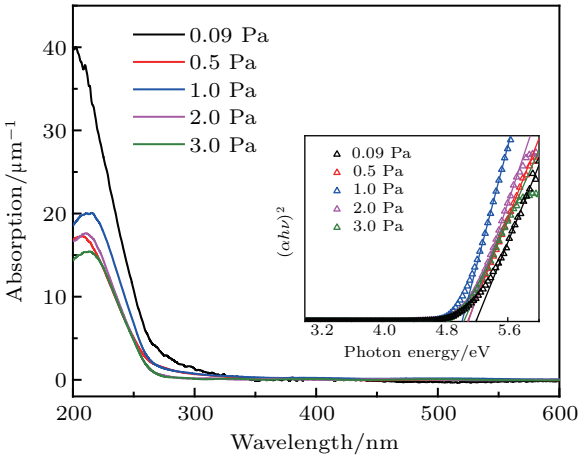


Fig. 5. UV–visible transmittance spectra of the Ga_2O_3 thin films grown at various oxygen pressures. The inset shows the plot of $(\alpha h\nu)^2$ versus $h\nu$ used to estimate the bandgap.

Figure 6 shows the spectroscopic photoresponsivity of the fabricated Ga_2O_3 SBPDs measured at a bias of 25.0 V at different wavelengths ranging from 200 nm to 600 nm, and the inset is a schematic diagram of the device structure of the SBPD. It is evident that the photoresponsivity exhibits a significant increase of approximately two orders of magnitude when the oxygen pressure decreases from 2.0 Pa to 1.0 Pa. Moreover, the photoresponsivity values of all mixed-phase Ga_2O_3 SBPDs are approximately two orders of magnitude higher than those of the single β-Ga_2O_3 SBPDs, and the photoresponsivity reaches a maximum of 12 A/W; the I_{light}/I_{dark} reaches a maximum of 191.3. Interestingly, the crystal structure of the Ga_2O_3 thin film changed from a single β phase to a mixed-phase when the oxygen pressure was reduced from 2.0 Pa to 1.0 Pa. As has been reported, the dangling bonds and interface states could cause a high internal gain that will lead to a high responsivity and a persistent photocurrent effect.[1,15] A detailed analysis, according to previous reports, is as follows. The responsivity (R) of photodetectors can be expressed as[34]

$$R = I_{ph}/P_{inc}, \tag{3}$$

$$I_{ph} = wtq\,(\Delta n\mu_e + \Delta p\mu_h)\,V_b/l, \tag{4}$$

where I_{ph} is the photocurrent; P_{inc} is the incident light power; w, t, and l are the width, thickness, and length of the interdigitated electrode, respectively; q is the electron charge; Δn and Δp are the minority electron and hole concentrations, respectively; μ_e and μ_h are the electron and hole mobilities, respectively; and V_b is the bias voltage.

Apparently, at a fixed bias voltage, the photoresponsivity of the UV detector is determined by the photocurrent, and the photocurrent is proportional to the number of carriers generated under illumination and their mobility. Furthermore, the number of carriers and their mobility are related to the UV absorption coefficient of Ga_2O_3 thin films and the ability of photocarriers to transmit in Ga_2O_3 thin films.[34] As shown in Fig. 5, the maximum value of the light absorption coefficients of different samples is approximately two times the minimum value, but the maximum value of the photoresponsivity of the samples is approximately two orders of magnitude higher than the minimum value. Therefore, the high responsivity of the mixed-phase Ga_2O_3 SBPDs can be ascribed to the high internal gain, which is caused by the large number of dangling bonds in the interfaces between the α and β phases in Ga_2O_3. The relationship between the responsivity (R) and internal gain (G) can be expressed as[1,15,33]

$$R = G\frac{q\lambda\eta}{\hbar c}, \tag{5}$$

where λ is the wavelength of the incident light, η is the quantum efficiency, $\hbar$ is Planck's constant, and c is the velocity of the incident light. Thus, assuming that the quantum efficiency is 100%, the incident photons are completely absorbed. The internal gain is proportional to the photoresponsivity.

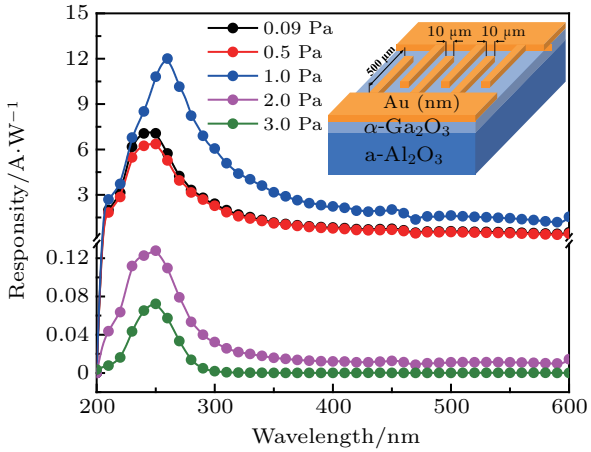


Fig. 6. Spectroscopic photoresponsivity of Ga_2O_3 SBPDs measured at a bias of 25.0 V at different wavelengths ranging from 200 nm to 600 nm. The inset is a schematic diagram of the fabricated Ga_2O_3 thin film MSM structure photodetector.

As mentioned above, there are a large number of dangling bonds in the mixed-phase Ga_2O_3 films, which cause a great number of heterojunction interfaces between monoclinic β-Ga_2O_3 and corundum α-Ga_2O_3. Theoretically, the many heterojunction interfaces are responsible for the high responsivity and low dark current of the photodetector devices.[15] Apparently, high-responsivity devices have been fabricated on mixed-phase Ga_2O_3 thin films, but unfortunately, an undesired high dark current has also been acquired. The detailed results are as follows. Table 1 shows a comparison of the I_{light}, I_{dark}, and I_{light}/I_{dark} for the devices with different oxygen pressures. Both the light and dark currents of the mixed-phase Ga_2O_3 SBPDs are approximately three orders of magnitude greater than those of the single β-Ga_2O_3 SBPDs. This phenomenon is likely caused by the large number of dangling bonds between monoclinic β-Ga_2O_3 and corundum α-Ga_2O_3, which

cause a high interface density. Furthermore, due to the dangling bonds, defects such as phase transformation dislocations are easily generated. These defects act as hole traps and can trap hole carriers, which would reduce the probability of recombination of non-balanced carriers and prolong carrier life; therefore, the light and dark currents of the devices are eventually larger. Another possible reason for this is that when the oxygen pressure in the cavity is low, the Ga_2O_3 thin film is in a gallium-rich and oxygen-deficient state. Furthermore, oxygen vacancies are generated in the film, and oxygen vacancies can provide free electrons as donor levels, and finally result in a higher dark current of the mixed-phase Ga_2O_3. Additionally, it can be seen that the dark current decreases slightly with a reduction in oxygen pressure, probably because the proportion of α-Ga_2O_3 increases and the proportion of β-Ga_2O_3 decreases. It must be noted that the I_{light}/I_{dark} of the device reaches 191.3 for the 1.0 Pa film, which is much higher than that of other mixed-phase Ga_2O_3 SBPDs with the 0.5 Pa and 0.09 Pa films. According to previous research results of our research group, the cause of this phenomenon is that the mixed-phase Ga_2O_3 thin film grown at 1.0 Pa mainly grows along (400) and $(\bar{2}01)$ planes, with the wider bandgap of (400) β-Ga_2O_3 and relatively high density of boundaries at the interfaces between the (400) and $(\bar{2}01)$ planes leading to a higher I_{light}/I_{dark}.[35]

Table 1. Comparison of I_{light}, I_{dark}, and I_{light}/I_{dark} for the devices with different oxygen pressures.

Oxygen pressure/Pa	Structure	I_{light}/A	I_{dark}/A	I_{light}/I_{dark}
3.0	β-Ga_2O_3	$7.25\times$	$2.39\times$	303.1
2.0		$3.01\times$	$5.04\times$	173.3
1.0		$6.03\times$	$1.78\times$	191.3
0.5	mixed-phase Ga_2O_3	$3.08\times$	$1.65\times$	55.2
0.09		$4.01\times$	$1.55\times$	39.2

To deeply investigate the response speed characteristics of the device, 266 nm wavelength light was used to illuminate the device, and a transient response time test was performed. Figure 7(a) shows the transient response of Ga_2O_3 SBPDs with various oxygen growth pressures at a bias of 25 V under 254 nm light illumination. We observed that the increment of the signal intensity was rapid when the excitation light was turned on. However, by turning off the excitation light, a relatively slow response occurred in the device. This slowly decaying response was ascribed to the oxygen-related hole trap states generated at the surface of the Ga_2O_3 thin film.[24] These hole trap states would reduce charge carrier recombination because some carriers are captured as the traps empty. Therefore, a slow decay time occurred when the incident light was turned off (Fig. 7(a)). Additionally, the rise time and decay time of the mixed-phase Ga_2O_3 SBPDs are longer than those of the single β-Ga_2O_3 SBPDs, as shown in Figs. 7(a) and 7(b). This is due to the high density of dangling bonds at the junction of α-Ga_2O_3 and β-Ga_2O_3 in the mixed-phase Ga_2O_3 thin film, and higher-density acceptor interface states can be introduced. These acceptor interface states can capture a large number of photogenerated holes and reduce the carrier recombination to prolong the lifetime of the photogenerated carriers.

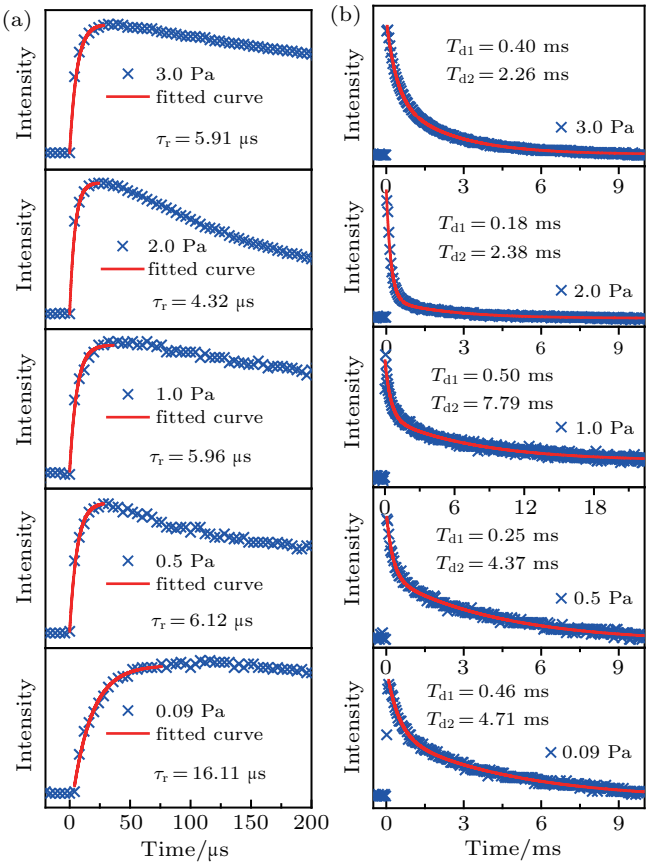


Fig. 7. The transient response of Ga_2O_3 SBPDs with various oxygen pressures at the bias of 25 V under 254 nm light illumination: (a) the drop time, and (b) the rise time.

4. Conclusion

In summary, Ga_2O_3 thin films were deposited on a-Al_2O_3 substrates by PLD with different oxygen pressures at 650 °C. By observing the XRD patterns and Raman spectra, it can be found that as the oxygen pressure in the chamber decreases from 3.0 Pa to 0.09 Pa, the crystal structure of the Ga_2O_3 thin film changes from a single β phase to mixed-phase. Due to the presence of a large number of dangling bonds at the interface of different internal structures of the mixed-phase Ga_2O_3 thin film, a high internal gain can be obtained, and therefore, the photoresponsivity can be greatly improved. The results of spectral responsivity tests show that the maximum responsivity of mixed-phase Ga_2O_3 SBPDs reached 12 A/W at a bias of 25 V, which is approximately two orders of magnitude higher than that of the single β-Ga_2O_3 SBPDs, with the response wavelength located at 260 nm. Additionally, the I_{light}/I_{dark}

reached two orders of magnitude higher in the mixed-phase than in the single β-phase Ga_2O_3. In fact, there is no denying that further effort should be focused on reducing the dark current and improving the response speed of the mixed-phase Ga_2O_3 SBPDs. The significance of our research work lies in the exploration of the feasibility of preparing a mixed-phase structure Ga_2O_3 film via the PLD method and further fabrication of a mixed-phase structure Ga_2O_3 thin film-type SBPD with excellent performance.

References

[1] Qian L X , Wu Z H , Zhang Y Y , Lai P T, Liu X Z and Li Y R 2017 *ACS Photon.* **4** 2203

[2] Guo X C, Hao N H, Guo D Y, Wu Z P, An Y H, Chu X L, Li L H, Li P G, Lei M and Tang W H 2016 *J. Alloys Compd.* **660** 136

[3] Cui S, Mei Z, Zhang Y, Liang H and Du X 2017 *Adv. Opt. Mater.* **5** 1700454

[4] Yu F P, Ou S L and Wuu D S 2015 *Opt. Mater. Express* **5** 1240

[5] Zhuo R, Wu D, Wang Y, Wu E, Jia C, Shi Z, Xu T, Tian Y and Li X 2018 *J. Mater. Chem. C* **6** 10982

[6] Zhuo R, Zeng L, Yuan H, Wu D, Wang Y, Shi Z, Xu T, Tian Y, Li X and Tsang Y H 2018 *Nano Res.*

[7] Zhuo R, Wang Y, Wu D, Lou Z, Shi Z, Xu T, Xu J, Tian Y and Li X 2018 *J. Mater. Chem. C* **6** 299

[8] Gökkavas M, Butun S, Tut T, Biyikli N and Ozbay E 2007 *Photonic. Nanostruct.* **5** 53

[9] Tut T, Biyikli N, Kimukin I, Kartaloglu T, Aytur O, Unlu M S and Ozbay E 2005 *Solid-State Electron.* **49** 117

[10] Soltani A et al 2008 *Appl. Phys. Lett.* **92** 053501

[11] Polyakov V I, Rukovishnikov A I, Avdeeva L A, Kun'kova Z E, Varnin V P, Teremetskaya I G and Ralchenko V G 2006 *Diamond Relat. Mater.* **15** 1972

[12] Polyakov V I, Rossukanyi N M, Krikunov A I, Varnin V P and Teremetskaya I G 1998 *Diamond Relat. Mater.* **7** 821

[13] Kaushal A and Kaur D 2009 *Sol. Energy Mater. Sol. Cells* **93** 193

[14] Teherani F H, Look D C, Rogers D J, Schoenfeld W V, Wei M, Boutwell R C and Liu H 2014 *Proc. of SPIE* **8987** 89871P

[15] Fan M M, Liu K W, Chen X, Wang X, Zhang Z Z, Li B H and Shen D Z 2015 *ACS Appl. Mater. Interfaces* **7** 20600

[16] Li G M, Zhang J W, Liu Y and Zhang K F 2011 *Opt. Eng.* **50** 113801

[17] Wang L K, Ju Z G, Zhang J Y, Zheng J, Shen D Z, Yao B, Zhao D X, Zhang Z Z, Li B H and Shan C X 2009 *Appl. Phys. Lett.* **95** 131113

[18] Kumar S S, Rubio E J, NoorA -Alam M, Martinez G, Manandhar S, Shutthanandan V, Thevuthasan S and Ramana C V 2013 *J. Phys. Chem. C* **117** 4194

[19] Roy R, Hill V G and F O E 1952 *J. Am. Chem. Soc.* **74** 719

[20] Zou R, Zhang Z, Liu Q, Hu J, Sang L, Liao M and Zhang W 2014 *Small* **10** 1848

[21] Oh S, Kim J, Ren F, Pearton S J and Kim J 2016 *J. Mater. Chem. C* **4** 9245

[22] Arnold S P, Prokes S M, Perkins F K and Zaghloul M E 2009 *Appl. Phys. Lett.* **95** 103102

[23] Guo D Y, Zhao X L, Zhi Y S, Cui W, Huang Y Q, An Y H, Li P G, Wu Z P and Tang W H 2016 *Mater. Lett.* **164** 364

[24] Weng W Y, Hsueh T J, Chang S J, Huang G J and Hsueh H T 2011 *IEEE Sens. J.* **11** 999

[25] He H, Orlando R, Blanco M A, Pandey R, Amzallag E, Baraille I and Rerat M 2006 *Phys. Rev. B* **74** 195123

[26] Gonzalez E A, Jasen P V, Juan A, Collins S E, Baltanás M A and Bonivardi A L 2005 *Surf. Sci.* **575** 171

[27] Seiler W, Selmane M, Abdelouhadi K and Perrière J 2015 *Thin Solid Films* **589** 556

[28] Tian W et al 2014 *Adv. Mater.* **26** 3088

[29] Han S, Shao Y K, Lu Y M, Cao P J, Jia F, Zeng Y X, Liu W J, Zhu D L and Ma X C 2013 *J. Alloys Compd.* **559** 209

[30] Rafique S, Han L, Neal A T, Mou S, Boeckl J and Zhao H 2018 *Phys. Status Solidi A* **215** 1700467

[31] Nikolaev V I, Pechnikov A I, Stepanov S I, Nikitina I P, Smirnov A N, Chikiryaka A V, Sharofidinov S S, Bougrov V E and Romanov A E 2016 *Mater. Sci. Semicond. Process.* **47** 16

[32] Tadjer M J et al 2016 *J. Electron. Mater.* **45** 2031

[33] Hu G C, Shan C X, Zhang N, Jiang M M, Wang S P and Shen D Z 2015 *Opt. Express* **23** 13554

[34] Razeghi M and Rogalski A 1996 *J. Appl. Phys.* **79** 7433

[35] Chen X H, Han S, Lu Y M, Cao P J, Liu W J, Zeng Y X, Jia F, Xu W Y, Liu X K and Zhu D L 2018 *J. Alloys Compd.* **747** 869